Semiconductor Science and Technology

PAPER

Single-trap emission kinetics of vertical β-Ga_2O_3 Schottky diodes by deep-level transient spectroscopy

To cite this article: Jiaxiang Chen *et al* 2021 *Semicond. Sci. Technol.* **36** 055015

IOP Publishing Semiconductor Science and Technology
Semicond. Sci. Technol. **36** (2021) 055015 (7pp) https://doi.org/10.1088/1361-6641/abed8d

Single-trap emission kinetics of vertical β-Ga_2O_3 Schottky diodes by deep-level transient spectroscopy

Jiaxiang Chen[1,2,3], Haoxun Luo[4], HaoLan Qu[1], Min Zhu[1,2,3], Haowen Guo[1], Baile Chen[1], Yuanjie Lv[5], Xing Lu[4,*] and Xinbo Zou[1,*]

[1] School of Information Science and Technology, ShanghaiTech University, 201210 Shanghai, People's Republic of China
[2] Shanghai Institute of Microsystem and Information Technology, Chinese Academy of Sciences, Shanghai 200050, People's Republic of China
[3] School of Microelectronics, University of Chinese Academy of Sciences, Beijing 100049, People's Republic of China
[4] School of Electronics and Information Technology, Sun Yat-sen University, Guangzhou 510275, People's Republic of China
[5] The National Key Laboratory of ASIC, Hebei Semiconductor Research Institute, Hebei 050051, People's Republic of China

E-mail: zouxb@shanghaitech.edu.cn and lux86@mail.sysu.edu.cn

Received 6 December 2020, revised 3 March 2021
Accepted for publication 10 March 2021
Published 8 April 2021

Abstract

We report the emission kinetics of a single-electron trap (E1, E_C–0.63 eV) in Sn-doped ($\bar{2}01$) β-Ga_2O_3 crystals studied using deeplevel transient spectroscopy (DLTS). The time constant (τ) of the electrons emitted from the trap level E1 was thoroughly investigated as a function of the temperature and the electric field (E-field) . The temperature-dependence τ of E1 was extracted by both the temperature-scanning and isothermal modes of DLTS. It was found that the emission process accelerated exponentially from 200 K to 350 K. The E-field dependence of the emission time constant could be divided into two regimes for all measurement steps (250–325 K). In the low-electric-field regime, the emission time constant of the trap decreased slightly with a strengthened E-field. With a further enhancement of the E-field ($E > 1.76$ MV cm^{-1}), the field-enhanced emission rate was accurately modeled by the Poole–Frenkel effect; the accelerated emission process was attributed to a reduction of the Coulomb well barrier for the donor-like trap E1.

Supplementary material for this article is available online

Keywords: Ga_2O_3, DLTS, Schottky diode, emission kinetics, single trap

(Some figures may appear in color only in the online journal)

1. Introduction

β-phase Ga_2O_3 has attracted considerable research interest for use in power conversion applications, due to its thermal stability, ultra-wide bandgap of 4.9 eV, and high critical breakdown electric field of 8 MV cm^{-1} [1, 2]. Various Ga_2O_3-based power devices, including metal–oxide–semiconductor field-effect transistors (FETs) [3, 4], metal–semiconductor FETs [5, 6], FinFETs [7] and Schottky barrier diodes (SBDs) [8–10] have been successfully demonstrated. In work toward reliable fast switching applications, the dynamic performance of Ga_2O_3-based devices has been measured and investigated.

* Authors to whom any correspondence should be addressed.

Forward conduction current loss after off-state stress [11] and reverse breakdown degradation after forward bias stress [12] have been reported for vertical Ga_2O_3 SBDs. After off-state stress, Zhang *et al* found that ion implantation-based edge termination could lead to worsened forward current drop, compared to the case without ion implantation, although the breakdown voltage was greatly improved [11]. It was suggested that the root cause of the above degradation was deep-level traps in the bulk materials [13–15]. Deep traps with energy levels 0.5, 0.6, 0.7, 0.8 and 1.0 eV below the conduction band minimum (CBM) have been commonly found in Ga_2O_3 manufactured by various growth methods and a number of characterization methods [16–18]. In particular, traps with activation energies of around 0.6 eV have been extensively identified and reported using various methods, including deep-level transient spectroscopy (DLTS) [16, 19]. Nevertheless, physical insight into the emission and capture mechanisms of this trap (E_C–0.6 eV) is still missing.

To achieve reliable high-power switching applications, it is necessary to understand the temperature-dependent and electric-field (E-field)-dependent characteristics of traps inside Ga_2O_3, particularly the characteristics related to the carrier trapping and de-trapping processes. Steady-state capacitance spectroscopy has been utilized to study the trap emission time constant (τ) of Ga_2O_3 SBD at, or slightly higher than, room temperature [20], but it was challenging to extract the time constant at temperatures well above room temperature. The isothermal DLTS method [21], which features multiple sampling time spans at fixed temperature steps, has been employed to obtain the short-emission-time constants (<1 s) of Ge-doped (010) Ga_2O_3 at temperatures of 405–430 K [22]. The influence of the electric field on the electron emission rate from deep levels can be generally modeled by three mechanisms: (a) the direct tunneling effect, (b) the Poole–Frenkel effect (PFE), and (c) phonon-assisted tunneling. The PFE, which is caused by a lowering of the Coulomb barrier, occurs for charged impurities only [23] whereas phonon-assisted tunneling (and direct tunneling in very strong electric fields) is possible for charged impurities in all charge states [24]. Field-enhanced emission behaviors have been reported for traps at temperatures above 360 K in molecular beam epitaxy- and hydride vapor phase epitaxy-grown β-Ga_2O_3 films, and a trap activation energy of 0.9–1 eV was revealed [18]. Phonon-assisted tunneling and PFE have been identified in edge-defined film-fed grown (EFG) Ga_2O_3 for trap levels at 0.8 eV and 1 eV below the conduction band, respectively [25].

Despite the steady advances in the understanding of trap properties in Ga_2O_3, two relevant issues still need to be addressed: (a) the trap emission time constants at or above room temperature have been reported, but were limited to a small temperature range (<30 K). The emission time constant mapping for a wide temperature range, e.g. 200–400 K is still unknown, which hinders a comprehensive understanding of its temperature dependence; (b) the electric-field-dependent emission mechanisms of traps with activation energies of 1 eV and 0.8 eV have been reported; however, the E-field dependent emission kinetics for shallower trap levels are not fully understood, in particular, for a range of temperatures.

In this paper, we describe an investigation of the device performance and single trap (E_C–0.63 eV) properties of EFG-based ($\bar{2}01$) β-Ga_2O_3 SBDs, in which temperature-dependent current–voltage (I–V) and capacitance–voltage (C–V) characterizations were performed, and two kinds of DLTS technique (temperature-scanning mode DLTS and isothermal mode DLTS) were used. To profile the trap location in the device and its origin, the reverse bias, pulse voltage and filling pulse width were varied in the DLTS temperature scan. Mapping of the effects of thermal acceleration on the trap emission process was performed using both DLTS techniques at a wide range of temperatures from 200 K to 350 K. A detailed study was made of the field-enhanced emission mechanisms of both the low-electric-field and high-electric-field regions.

2. Device structural and electrical characterizations

The inset of figure 1(a) shows a schematic cross-section of the vertical β-Ga_2O_3 SBD used in this study. A ($\bar{2}01$) β-Ga_2O_3 wafer was prepared by EFG method with a thickness of 600 μm and a top Sn:Ga_2O_3 layer electron concentration of around 2.3×10^{17} cm^{-3}. The vertical diode structure was fabricated using Ni/Au for the Schottky contact and Ti/Au for the ohmic contact. At 300 K, the turn-on voltage was measured to be 0.82 V (using 1 A cm^{-2} as the threshold current criteria) and the specific on-resistance (R_{on}) was about 22.3 mΩ cm^2 at a current density of 50 A cm^{-2}. The turn-on voltage increased from 0.75 V to 0.96 V as the temperature decreased from 350 K to 200 K, and the corresponding R_{on} decreased from 24.2 to 21.3 mΩ cm^{2}at 50 A cm^{-2} owing to higher mobility at a lower temperature [26, 27]. For the same temperature range, the leakage current density was greatly suppressed from 1.5×10^{-3} A cm^{-2} down to 3.5×10^{-4} A cm^{-2} at -50 V with decreasing temperature, indicating the enhanced DC performance of the device at lower temperatures. Although no advanced passivation technique was applied, the leakage current level was comparable with the state-of-the-art β-Ga_2O_3 SBDs described in the literature [8, 28].

Figure 1(c) shows a $1/C^2$–V plot from 200 K to 350 K; the net donor concentration (N_S) of the SBD extracted from the capacitance–voltage (C–V) measurements was 2.3×10^{17} cm^{-3} at 300 K. The Schottky barrier height (SBH) was extracted from the C–V characteristics at various temperatures, taking image-force-induced barrier height lowering into account [29]:

$$q\emptyset_B = qV_{bi} + E_C - E_F - q\emptyset_{IFL} \quad (1)$$

where $\emptyset_B$ is the SBH, E_C is the CBM of Ga_2O_3, E_F is the Fermi level, q is the elementary charge, and $\emptyset_{IFL}$ is the image-force-induced barrier height lowering. The value of the potential barrier height (qV_{bi}) monotonically decreased from 1.38 eV to 1.24 eV when the temperature increased from 200 K to 350 K. Accordingly, the SBH reduced from 1.42 eV to 1.34 eV, which was a good match for the decrease in the threshold voltage of the SBD when the temperature was raised.

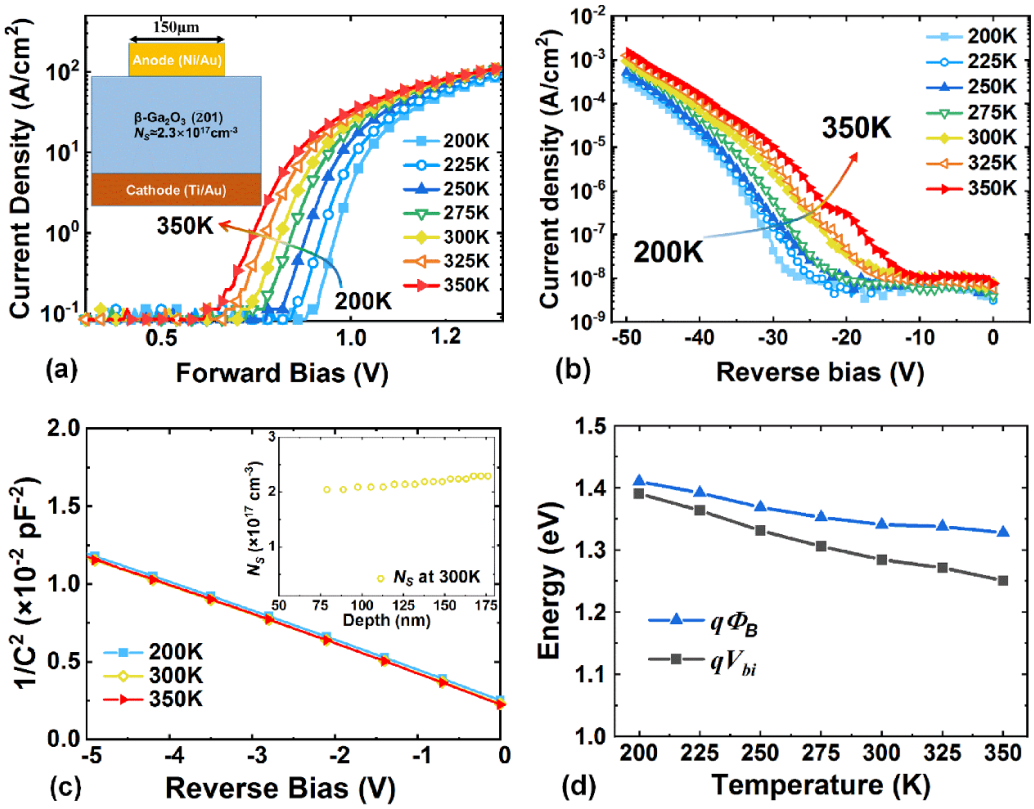

Figure 1. (a) Forward I–V characteristics in the temperature range of 200–350 K. Inset: schematic of the vertical β-Ga_2O_3 SBD fabricated. (b) Reverse I–V characteristics. (c) $1/C^2$–V characteristics at 1 MHz. Inset: the net donor concentration (N_S) of the device was extracted from C–V measurements. (d) The temperature-dependent built-in potential (V_{bi}) and Schottky barrier height (SBH) extracted from a linear extrapolation of the C–V measurements.

3. DLTS results and discussion

Figure 2(a) shows the temperature-scanning mode DLTS signal spectra scanned from 200 K to 350 K with a reverse bias $U_R = -8$ V, a filling pulse height $U_P = -0.1$ V, and a filling pulse width $t_P = 1$ ms. Using maxima and Laplace analyses [30, 31], we identified one majority carrier (electron) trap, called E1 ($E_C-0.63$ eV) with a capture cross-section $\sigma_n = 3.07 \times 10^{-17}$ cm^2, as shown in Figure 2(b). The E1 trap concentration (N_T) was 9.5 $\times 10^{15}$ cm^{-3}. This trap energy level has been widely observed in Ga_2O_3 devices grown by either the EFG [16, 19] or Czohralski (CZ) methods [32, 33], and the origin of E1 was thought to be associated with point defects [16, 34]. Compared to the trap level of $E_C-0.62$ eV with a N_T of 4.7 $\times 10^{14}$ cm^{-3} in the previously reported un-doped (010) Ga_2O_3 [16], the trap concentration of E1 in this Sn-doped sample is higher by one order of magnitude.

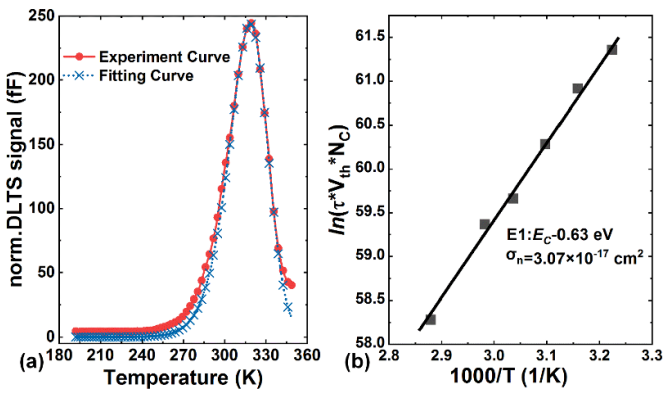

Figure 2. (a) Temperature-scanning-mode DLTS spectrum of a Ga_2O_3 SBD from 200 K to 350 K and its fitting curve. (b) Arrhenius plot of the deep trap level known as E1.

Figure 3(a) shows the DLTS signal collected by varying the filling pulse width (t_P) from 10 μs to 1 ms. Despite the filling pulse width variation, the DLTS signal curves were typically identical to each other, which indicated that the time taken to fully fill the traps was less than 10 μs and that further increasing the filling time would not help to amplify the signal. The uniform results also implied that the origin of E1 was associated with point defects, rather than extended defects [16, 34, 35]. Figure 3(b) shows a quenching of the DLTS peak amplitude when the filling pulse voltage (U_P) amplitude was increased from -0.1 V to -5 V while keeping the reverse bias (U_R) and t_P unchanged. The lowering of the DLTS signal corresponded to a reduction of the sampled volume. For the same reason, when changing the reverse bias from -0.5 V to -8 V while keeping $U_P = -0.1$ V and $t_P = 1$ ms, the probed region became deeper in the Ga_2O_3 device (from the surface). Thus, we were able to detect defects from the surface

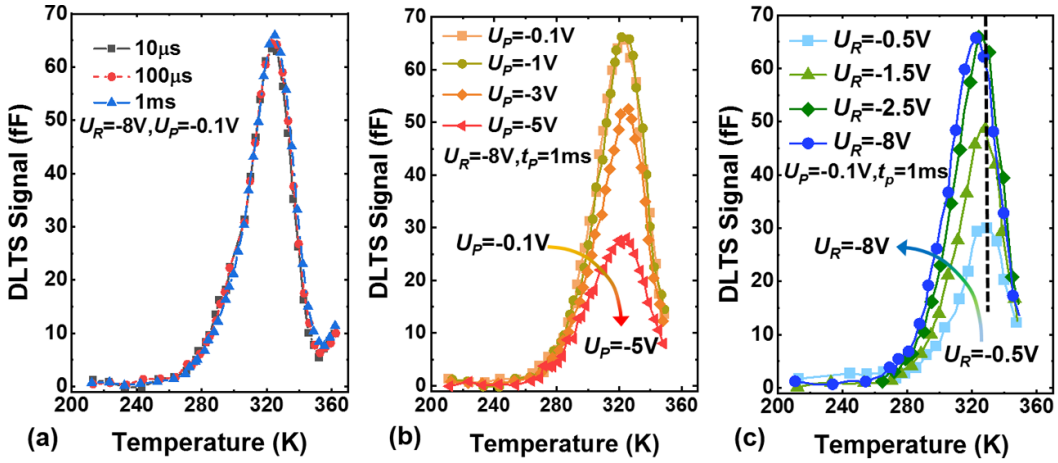

Figure 3. DLTS spectrum of Ga_2O_3 as a function of (a) the filling pulse width (b) the filling pulse voltage and (c) the reverse bias (the vertical dashed line is a guide for the eye).

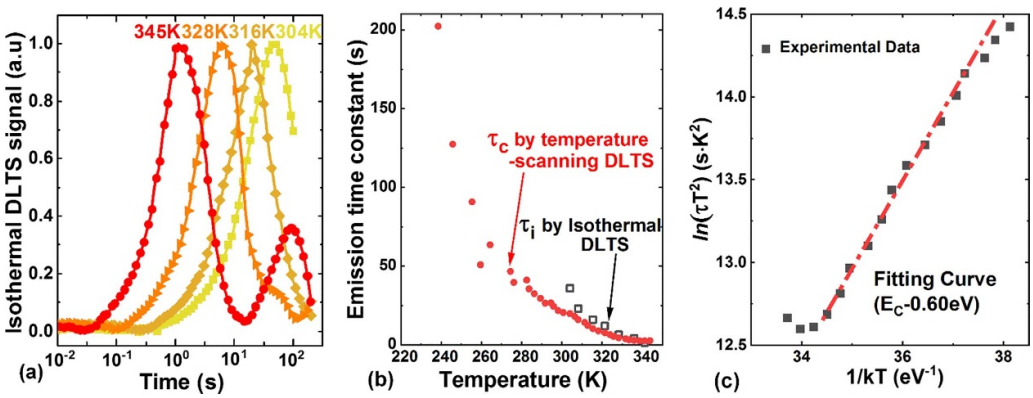

Figure 4. (a) Representative DLTS signals at four measurement temperatures. (b) Temperature dependence of τ_i and τ_c by isothermal DLTS and temperature-scanning DLTS ($U_R = -8$ V, $U_p = -0.1$ V, and $t_p = 1$ ms). (c) Data points fitted to temperature dependence, τ_c.

to the bulk of the Ga_2O_3 layer at various depths. As shown in figure 3(c), when the reverse bias voltage increased, the DLTS signal amplitude became higher, indicating that the number of traps involved in the transient capacitance measurement had increased. Hence, the traps are thought to be mainly located in the bulk Ga_2O_3 layer rather than interface-related [35, 36]. In addition, it should be noted that the peak position shifted in the direction of lower temperatures when the reverse bias amplitude increased, indicating that reverse bias exerted an influence on the trap emission rate, [37] which would be further discussed in the E-field-related session (figure 5).

Figure 4(a) shows the normalized isothermal-mode DLTS signal as a function of time for four fixed temperature levels. More detailed isothernal-mode DLTS information can be found in supplementary material (availabe online at stacks.iop.org/SST/36/055015/mmedia).

With increasing temperature, the main peak that denotes the trap level of $E_C-0.63$ eV exhibits smaller time constants, as shown in figure 4(b). The time constant extracted from the main peaks of the isothermal DLTS signal (τ_i) decreased from 36.8 s to 1.4 s when the temperature increased from 304 K to 345 K. Figure 4(b) also shows the temperature-dependent emission time constant (τ_c) extracted by the temperature-scanning method for comparison. The τ_c was greatly reduced from 202.4 s at 235 K to 2.6 s at 345 K, indicating that raising the temperature indeed accelerated the emission process [20]. Meanwhile, the time constants extracted by the two methods are a good match for each other.

The temperature-dependent relationship was also re-plotted in figure 4(c). It was found that the emission time constant maintained an exponential relationship with temperature, which can be fitted by the Arrhenius relation, assuming a degeneracy ratio of 1, as shown in equation (2) [38]:

$$\ln\left(\tau T^2\right) = \frac{E_C - E_T}{kT} - \ln\left(\gamma\sigma_n\right) \tag{2}$$

where k is the Boltzmann constant, γ is the characteristic constant related to the effective mass of the electron, E_T is the trap energy and σ_n is the capture cross-section.

From the slope and intercept of the data points above 300 K (red fitting line in figure 4(c)), an activation energy of 0.60 eV and a capture cross-section of 1.08×10^{-17} cm^2 were extracted, respectively. The results are a good match for the trap energy level extracted in figure 2, confirming that it is E1 that governs the trap emission behavior. It is also noted that a second peak starts to appear at a temperature of 345 K (figure 4(a)), corresponding to a deeper energy level beyond

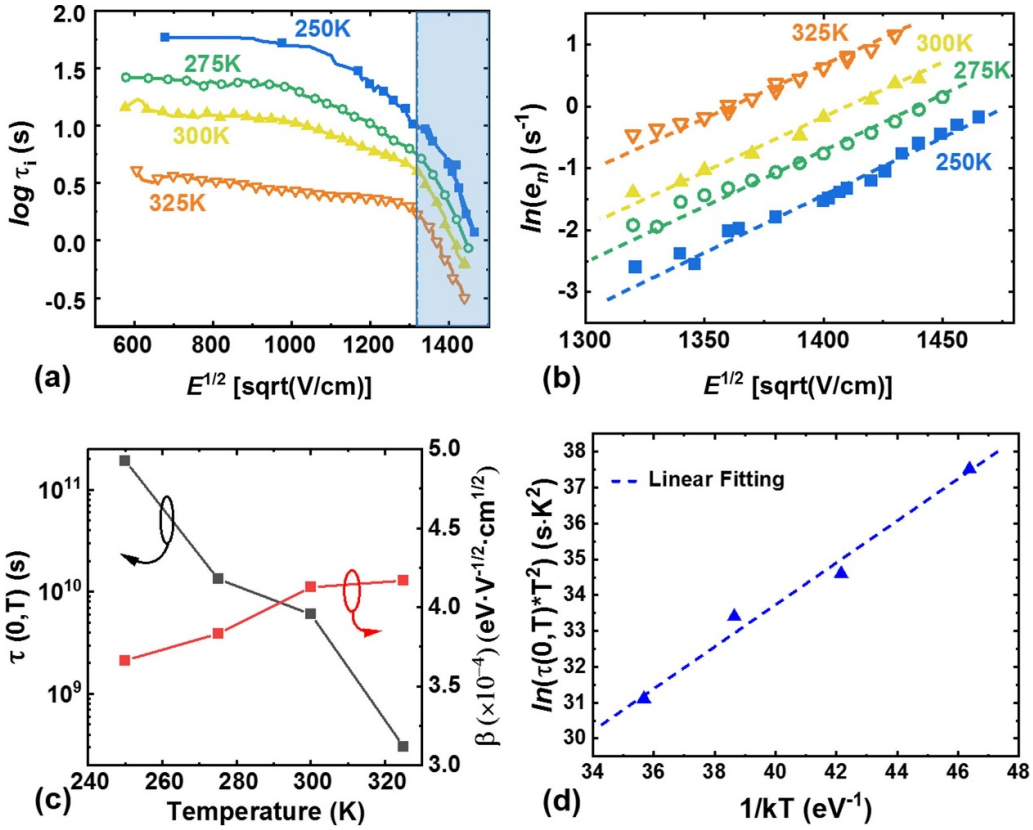

Figure 5. (a) Electric-field-dependent emission time constants extracted by DLTS. (b) Electric-field-dependent emission rate versus the square root of the electric field at various temperatures. (c) Extracted $\tau(0, T)$ and β_{PF} as a function of temperature. (d) Arrhenius plot of $\tau(0, T)$ at four temperatures.

0.63 eV which, however, is outside the scope of this study and needs further investigation at higher temperatures.

Figure 5(a) shows the emission time constants measured under reverse bias (0 V to −50 V) at four fixed temperatures from 250 K to 325 K. For all the temperature steps, the values of τ_i were reduced by a strengthening electric field. Based on the PFE signature of linear $\ln(e_n)$ versus $E^{1/2}$ [24], two regions have been identified: a relatively low electric field region ($E^{1/2} < 1325$ (V cm^{-1})$^{1/2}$—the unshaded region in figure 5(a)), and a relatively high electric field region ($E^{1/2} > 1325$ (V cm^{-1})$^{1/2}$—the shaded region). In the low-field range, the emission time constants only slightly decreased when the E-field increased. At 325 K, the emission time constant was 3.9 s at $E = 3.67 \times 10^5$ V cm^{-1} ($E^{1/2} = 606$ (V cm^{-1})$^{1/2}$), which dropped to 0.3 s at $E = 2.07$ MV cm^{-1} ($E^{1/2} = 1440$ (V cm^{-1})$^{1/2}$).

In the relatively large electric field range (figures 5(a) and (b)), the emission rate was clearly accelerated by the electric field. It is noted that the emission rate (e_n) is linearly proportional to the square root of the electric field for all temperature steps (figure 5(b)). The electric field dependence of the electron emission rate from the trap level indicates that PFE [23] was the governing mechanism when $E^{1/2}$ was higher than 1325 (V cm^{-1})$^{1/2}$. A comprehensive model describing the thermal and E-field contributions to electrons emission from the trap state follows [39, 40]:

$$\ln e_n(E,T) = \ln\left(\tau(0,T)^{-1}\right) + \left(\frac{\beta_{PF}}{kT}\right)E^{1/2} \qquad (3)$$

where $e_n(E, T)$ (reciprocal of τ) represents the temperature and E-field-dependent electron emission rate; $\tau(0, T)$ is the emission time constant at a zero electric field at various temperatures and is the reciprocal of $e_n(0, T)$, E is the maximum electric field at the Schottky interface and can be expressed as $E = \sqrt{2qN_S(V_{bi} - V)/\varepsilon_s\varepsilon_0}$ [29]. Figure 5(c) shows the extracted $\tau(0, T)$ and β_{PF} (Poole–Frenkel coefficient) as a function of temperature from 250 K to 325 K. Here, $\tau(0, T)$ was found to be extremely long when no E-field was applied, and that the purely temperature-induced emission effect was shown to remain weak. Based on the slopes of the curves in figure 5(b), β_{PF} was found to increase slightly with an increase in temperature and was comparable to the value of 3.45×10^{-4} eV V$^{-1/2}$ cm$^{1/2}$ observed for GaN [41]. Given a nearly constant β_{PF}, the acceleration of the emission rate as a result of the applied E-field can be associated with and explained by the reduction of the Coulomb well barrier, which is described by $\beta_{PF}E^{1/2}$. The electric-field dependence of the trap emission rate, described by the PFE model, also indicated that E1 is a donor-like trap [42] in the n-type Ga_2O_3 material. The activation energy was extracted from $\tau(0, T)$ as a function of temperature in figure 5(c) via equation (2). The Arrhenius plot and linear fit of $\tau(0,T)$ are shown in figure 5(d).

An activation energy of 0.58 ± 0.03 eV was obtained from the slope, in good agreement with the trap energy level of $E_C-0.63$ eV obtained by temperature-scanning mode DLTS (figure 2). It should also be noted that the leakage current of the diode was still sufficiently low over a relatively large reverse bias range (-25 V < Vr < -50 V). The effective activation energy of the leakage current was shown to be above 1 eV, much higher than the studied trap level of $E_C-0.63$ eV, so that leakage current effects were ruled out from the DLTS spectra. The capacitive DLTS signals collected could reasonably represent single trap behavior without being distorted by leakage conduction, in either the temperature-scanning mode or the isothermal mode.

4. Conclusions

In summary, the temperature dependent *I–V* and *C–V* characteristics of a vertical β-Ga_2O_3 SBD were analyzed from 200 K to 350 K. The deep-level E1 ($E_C-0.63$ eV) was observed using conventional temperature-scanning mode DLTS and isothermal mode DLTS methods. The temperature-dependent and electric-field-dependent emission kinetics of the E1 trap were investigated, showing that the emission process was accelerated by increasing the temperature and/or applying a higher electric field. The trap parameters extracted from the emission time constant plot were a good match for the trap information revealed by the temperature-scanning mode DLTS. The analysis of the electric-field-dependent trap emission kinetics took the field level into account, in addition to the impact of temperature. For the relatively low field range, the emission time was found to slightly decrease with an increase in the E-field. In the relatively high field range, the field-enhanced emission time can be accurately modeled by the PFE when $E^{1/2}$ is higher than 1325 $(\mathrm{V\ cm^{-1}})^{1/2}$.

Data availability statement

All data that support the findings of this study are included within the article (and any supplementary files). Data will be available from 10 March 2021.

Acknowledgments

This work was supported in part by ShanghaiTech University Startup Fund, in part by the Shanghai Pujiang Program under Grant 18PJ1408200, and in part by the Shanghai Eastern Scholar (Youth) Program.

ORCID iDs

Baile Chen https://orcid.org/0000-0002-3265-5787
Yuanjie Lv https://orcid.org/0000-0002-9207-8344
Xing Lu https://orcid.org/0000-0001-5808-9552
Xinbo Zou https://orcid.org/0000-0002-9031-8519

References

[1] Higashiwaki M, Sasaki K, Murakami H, Kumagai Y, Koukitu A, Kuramata A, Masui T and Yamakoshi S 2016 *Semicond. Sci. Technol.* **31** 034001
[2] Galazka Z 2018 *Semicond. Sci. Technol.* **33** 113001
[3] Pearton S, Ren F, Tadjer M and Kim J 2018 *J. Appl. Phys.* **124** 220901
[4] Green A J *et al* 2016 *IEEE Electron Device Lett.* **37** 902–5
[5] Pearton S, Yang J, Carey P, Ren F, Kim J, Tadjer M and Mastro M 2018 *Appl. Phys. Rev.* **5** 011301
[6] Chabak K D *et al* 2019 *Semicond. Sci. Technol.* **35** 013002
[7] Chabak K *et al* 2016 *Appl. Phys. Lett.* **109** 213501
[8] Li W, Saraswat D, Long Y, Nomoto K, Jena D and Xing H 2020 *Appl. Phys. Lett.* **116** 192101
[9] Wang B, Xiao M, Yan X, Wong H, Ma J, Sasaki K and Wang H 2019 *Appl. Phys. Lett.* **115** 263503
[10] Jayawardena A, Ahyi A C and Dhar S 2016 *Semicond. Sci. Technol.* **31** 115002
[11] Zhang Y, Zhang J, Feng Z, Hu Z, Chen J, Dang K, Yan Q, Dong P, Zhou H and Hao Y 2020 *IEEE Trans. Electron Devices* **67** 3948–53
[12] Xian M, Elhassani R, Fares C, Ren F, Tadjer M and Pearton S 2019 *J. Vac. Sci. Technol.* B **37** 061205
[13] Ma J, Lee O and Yoo G 2018 *IEEE J. Electron Devices Soc.* **6** 1124–8
[14] Fabris E *et al* 2020 *IEEE Trans. Electron Devices* **67** 3954–9
[15] Kaushik J K, Balakrishnan V R, Mongia D, Kumar U, Dayal S, Panwar B S and Muralidharan R 2016 *Thin Solid Films* **612** 147–52
[16] Zhang Z, Farzana E, Arehart A R and Ringel S A 2016 *Appl. Phys. Lett.* **108** 052105
[17] Irmscher K, Galazka Z, Pietsch M, Uecker R and Fornari R 2011 *J. Appl. Phys.* **110** 063720
[18] Ingebrigtsen M, Kuznetsov A, Svensson B, Alfieri G, Mihaila A and Vines L 2019 *J. Appl. Phys.* **125** 185706
[19] Lin Y-Y, Neal A T, Mou S and Li J V 2019 *J. Vac. Sci. Technol.* B **37** 041204
[20] Huang S-S, Lopez R, Paul S, Neal A T, Mou S, Houng M-P and Li J V 2018 *Japan. J. Appl. Phys.* **57** 091101
[21] Zhang Y, Zhang X, Zhu M, Chen J, Tang C W, Lau K M and Zou X 2020 *IEEE Trans. Electron Devices* **67** 3992–8
[22] Farzana E, Ahmadi E, Speck J, Arehart A and Ringel S 2018 *J. Appl. Phys.* **123** 161410
[23] Zaidi M A, Bourgoin J C and Maaref H 1989 *Semicond. Sci. Technol.* **4** 739–42
[24] Coelho A V P and Boudinov H 2008 *Phys. Rev.* B **77** 235210
[25] Polyakov A Y, Lee I-H, Smirnov N B, Shchemerov I V, Vasilev A A, Chernykh A V and Pearton S J 2020 *J. Phys. D: Appl. Phys.* **53** 304001
[26] Ma N, Tanen N, Verma A, Guo Z, Luo T, An H, Xing H and Jena D 2016 *Appl. Phys. Lett.* **109** 212101
[27] Chen J, Zhu M, Lu X and Zou X 2020 *Appl. Phys. Lett.* **116** 062102
[28] Hu Z *et al* 2020 *ECS J. Solid State Sci. Technol.* **9** 025001
[29] Higashiwaki M *et al* 2016 *Appl. Phys. Lett.* **108** 133503
[30] Dobaczewski L, Kaczor P, Hawkins I and Peaker A 1994 *J. Appl. Phys.* **76** 194–8
[31] Rosenberg J, Legodi M, Rakita Y, Cahen D and Diale M 2017 *J. Appl. Phys.* **122** 145701
[32] Wang B, Look D and Leedy K 2019 *J. Appl. Phys.* **125** 105103
[33] Islam M M, Rana D, Hernandez A, Haseman M and Selim F 2019 *J. Appl. Phys.* **125** 055701
[34] Polyakov A, Smirnov N, Schemerov I, Yakimov E, Yang J, Ren F, Yang G, Kim J, Kuramata A and Pearton S 2018 *Appl. Phys. Lett.* **112** 032107
[35] Heo S *et al* 2016 *Sci. Rep.* **6** 30554
[36] Cho H, Kim C-S and Hong C H 2003 *J. Appl. Phys.* **94** 1485–9

[37] Coelho A, Adam M and Boudinov H 2011 *J. Phys. D: Appl. Phys.* **44** 305303
[38] Nguyen S, Lin K, Fitzgerald E and Chua S 2015 *Appl. Phys. Lett.* **106** 102101
[39] Kimerling L and Benton J 1981 *Appl. Phys. Lett.* **39** 410–2
[40] Hill R 1971 *Phil. Mag.* **23** 59–86
[41] Musolino M, van Treeck D, Tahraoui A, Scarparo L, Santi C, Meneghini M, Zanoni E, Geelhaar L and Riechert H 2015 *J. Appl. Phys.* **119** 044502
[42] Goodman S A, Auret F D, Koschnick F, Spaeth J M, Beaumont B and Gibart P 1999 *Appl. Phys. Lett.* **74** 809–11